2020-08

Predicting beach rotation using multiple atmospheric indices

Wiggins, Mark

10.1016/j.margeo.2020.106207
Marine Geology
Elsevier BV

Predicting beach rotation using multiple atmospheric indices

Mark Wiggins[1], Tim Scott[1], Gerd Masselink[1], R. Jak McCarroll[1] & Paul Russell[1]

1. *Coastal Processes Research Group, Plymouth University, Drake Circus, Plymouth PL4 8AA, United Kingdom.*

Corresponding author: Mark Wiggins. mark.wiggins@plymouth.ac.uk

Abstract

Shoreline change in the form of beach rotation can occur at event to decadal timescales, especially in semi-sheltered embayments with bi-directional wave climates, leading to enhanced coastal vulnerability under predictions of increased sea level rise. Previous studies have shown that phases of winter-averaged atmospheric indices in the North Atlantic correlate with variations in average winter wave height and dominant direction; however, predictions of a localised wave climate and beach rotation from individual climate indices has exhibited limited skill. Here we show that the combination of two major north Atlantic climate indices, the North Atlantic Oscillation (NAO) and West Europe Pressure Anomaly (WEPA), improves the prediction of a wave power directionality index (WDI), known to correlate with beach rotation along the length of a headland bound gravel embayment. Results using a combination of NAO and WEPA, improves predictions of WDI with an associated R^2 of 0.66, when compared to 0.23 and 0.31 for NAO and WEPA individually. Hindcast ($WDI_{WW3)}$ and index predicted (WDI_{Pred}) values of the WDI were shown to validate against measured beach rotation from 2008 to 2018 and modelled inshore potential longshore energy fluxes from 1980 to 2018. A long-term historic time series of WDI_{Pred} (1906-present) was then hindcast using records of NAO and WEPA. Qualitative validation of long-term beach rotation in response to the WDI_{Pred} is achieved with proxy records of beach change in the form of oblique and aerial photography and topographic maps. Low frequency (~60

years) beach rotation is shown to follow phases of the detrended cumulative WDI_{Pred} values, over the period of 1906 to 2018, linked to the multi-decadal fluctuations in detrended cumulative values of NAO and WEPA. When examined in the context of millennial-scale proxy NAO records, it is clear the recent centurial-scale analysis does not capture past variability and duration. This work has shown that: (1) potential future season ahead forecasts of atmospheric indices may skilfully predict beach rotation in many regions with bi-directional wave climates; and (2) historical analysis highlights the potential past phases of extreme coastal realignment. These new insights will lead to proactive and informed management from local authorities and coastal engineers.

Keywords: Beach rotation, NAO, WEPA, climate indices, atmospheric variability, N Atlantic.

1. Introduction

Predicting shoreline change and evolution is an ever growing issue for coastal managers, engineers and communities, particularly in light of observed and forecasted sea level rise (Nicholls et al., 2011). Whilst increases in storminess and significant wave height (Dodet et al., 2010) have been shown to cause significant cross-shore erosion of exposed beaches (Burvingt et al., 2016; Masselink et al., 2016; Scott et al., 2016), beach rotation due to longshore sediment transport under changes in the incoming wave direction (Klein et al., 2002), plays an equally important role in coastal vulnerability for many semi-sheltered embayments with bi-directional wave climates (Ruiz de Alegria-Arzaburu and Masselink, 2010; Wiggins et al., 2019a). Single storm events and annual winter rotational responses can leave embayments depleted of sediment at the up-wave extent, reducing overall beach volume and increasing the risk of damage, flooding and cliff retreat. If the wave climate maintains a bias towards a particular direction over multi-annual to decadal timescales, these

potential risks increase, due to the lack of recovered beach volumes, reducing the protection offered against damage under storm wave attack.

Understanding the controls that wave power and direction have on beach response has been investigated globally, with phases of atmospheric indices showing strong links to wave height and direction on local to basin wide scales (Barnard et al., 2015; Harley et al., 2017; Ranasinghe et al., 2004). Within the North Atlantic, recent studies have identified both the North Atlantic Oscillation (NAO) and West Europe Pressure Anomaly (WEPA) as playing a significant role in controlling both the winter-averaged wave height and dominant wind directions (Bacon and Carter, 1993; Castelle et al., 2018, 2017; Dodet et al., 2010; Izaguirre et al., 2010; Martínez-Asensio et al., 2016; Plomaritis et al., 2015). Positive phases of the NAO have been shown to predict increased winter wave height and westerly winds in the upper latitudes of the north Atlantic, northward of 52° N, whilst positive phases of WEPA outscore other indices in predicting increased wave heights southward of this latitude, until the coast of Portugal (Castelle et al., 2018). Along the entire length of the south coast of the United Kingdom (<52° N), where waves are directionally bi-modal (south-westerly and easterly), Wiggins et al. (2019b) observed that winter NAO and WEPA were best suited to predicting easterly and south-westerly winter-averaged wave power, respectively, with weak or no correlation in their opposite directions. In turn, the beach response for many south-east facing beaches along the same coastline, showed rotation was controlled by the Wave Directional Index (WDI), defined as the standardised winter power balance between the primary and secondary winter wave directions (Wiggins et al., 2019a). Despite the strong correlations between WDI and beach rotation, individually, NAO and WEPA were only weakly positively correlated with the WDI, and only significantly correlated with beach rotation in two of the 22 measured locations.

Given the current state of winter NAO forecasting (Dunstone et al., 2016; Scaife et al., 2015; Weisheimer et al., 2017), and the ability to predict several months ahead for the coming winter season, any improvements to our understanding of the relationship between atmospheric indices and morphology could lead us towards season ahead beach response forecasts for rotational sites, a tool that would be welcomed by coastal managers from local to regional scales. Furthermore, an improved relationship between climate variability and beach response could offer the capability to investigate historic beach state, providing a representative indicator of potential future variability, and place the observed contemporary changes into a longer-term context. For example, centurial-scale reconstructions of the NAO (Cook et al., 2002; Faust et al., 2016; Trouet et al., 2012) and the use of proxy records to model the NAO as far back as 3000BP (e.g. Baker et al., 2015), suggest that low frequency fluctuations of significant magnitude have occurred over multi-centurial timescales, many of which have been linked to well documented climate anomalies (e.g. Mediaeval Climate Anomaly, Little Ice Age), causing variations in precipitation, temperature and storminess, potentially driving large scale morphological activity such as sustained coastal dune transgression (Clarke and Rendell, 2006; Jackson et al., 2019). This study aims to investigate whether an improved relationship between climatic indices and winter WDI can be obtained by multivariate analysis, helping to place our current observations of wave climate controls on beach rotation into context with centurial scale fluctuations, allowing for proactive decisions in terms of long-term planning and coastal management.

2. Regional setting

Start Bay lies along the south coast of Devon, United Kingdom (50.27° N, 3.65° W), facing south east into the English Channel. The embayment consists of four interconnected coarse gravel barriers (D_{50} = 2 - 10mm), backed by freshwater lagoons and separated at high tides by protruding rocky headlands and wave cut platforms. Aligned from south-west to north-east,

its wave climate is bi-directional, consisting of predominantly diminished Atlantic swell waves from the south-west and short fetch easterly wind waves from the English Channel. Offshore wave angles are modulated by the presence of Skerries Bank (McCarroll et al., 2020) and Start Point (Figure 1), which refract and attenuate south-westerly waves to become southerly at the shoreline, whilst easterly waves maintain their angle as they propagate into the bay.

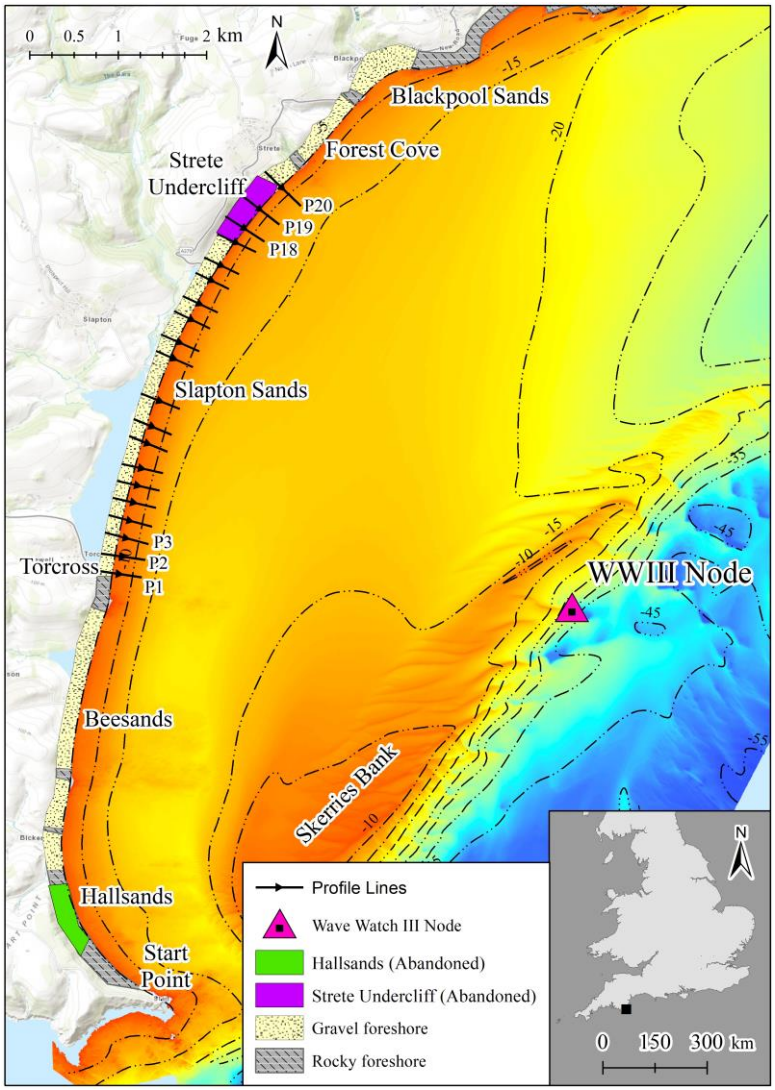

Figure 1. Location map of Start Bay with bathymetric contours (UKHO, 2013) and WWIII (Met Office) model node location. Topographic profile survey line locations are displayed as black arrows. The locations of two abandoned villages are displayed by the coloured polygons located towards the northern and southern ends of the embayment.

The southerly and easterly wave angles drive northward and southward sediment transport respectively, and the embayment is continually in a state of dynamic equilibrium, with the planform shape rotating in response to the current wave approach. The full embayment sediment cell as a whole, was demonstrated to be closed by Wiggins et al. (2019a), bounded by significant northern and southern headlands; however, beach rotation and exchange of sediment between the individual sub-embayments was observed through headland bypassing under extreme wave conditions (McCarroll et al., 2019) and sustained periods of a particular wave direction (Wiggins et al., 2019a).

Both full-embayment and sub-embayment beach rotation has long been a concern within Start Bay, with significant historical and contemporary examples being the subject of numerous scientific studies (Chadwick et al., 2005; Hails, 1975; McCarroll et al., 2019; Robinson, 1961; Ruiz de Alegria-Arzaburu and Masselink, 2010; Wiggins et al., 2019a, 2019b, 2017). The loss of the old village of Hallsands in 1917 is one of the highest profile cases of coastal erosion impacts in the United Kingdom. Lying at the southern corner of Start Bay (Figure 1), its collapse into the sea during a severe easterly storm followed a sustained lowering of the beach level in the years earlier, largely attributed to the dredging of subtidal beach material between 1897 and 1902 (Worth (1904), cited in May and Hansom (2003)). In addition to the dredging, evidence suggests that beach lowering at this end of the embayment was exacerbated due to a coincidental shift in winter NAO to a sustained positive phase for almost 30 years from the commencement of dredging (1898), leading to increased southerly waves, and clockwise rotation of the beach under prolonged northward sediment transport (Wiggins et al., 2017). Historical accounts of an earlier lost village at the opposite end of Start Bay, suggests the local community may have formed settlements based on the rotation and planform of the beach. Strete Undercliff, a small fishing village formed during the early 17th century (Goodall, 2007) and located at the northern end of Slapton Sands (Figure 1), was

documented on early nautical maps (Denbigh, 2017), until its subsequent disappearance by 1780 (Stranack, 2017; Waterhouse, 2009), around the time the village of Hallsands (in the south) became more established. Despite the lack of quantitative data from this period, it could be suggested that due to the closed nature of the sediment budget within Start Bay (Wiggins et al., 2019a), variations in multi-decadal phases of wave direction may have influenced the settlement locations of the past and present communities of Start Bay.

More recently, during the winter of 2013/14, Start Bay's beaches experienced significant clockwise rotation under a single winter season characterized by unprecedented south-westerly storm events (Masselink et al., 2015; Scott et al., 2016; Wiggins et al., 2019a), leaving the southern ends of embayments depleted of sediment. This increased the vulnerability of coastal defences at southern beach extremities, and in the following winter years (2015 and 2016), lack of beach volume resulted in the undermining and collapse of sea walls at Torcross, Slapton Sands, and loss of infrastructure including the car park at Hallsands (BBC, 2016).

3. Materials and methods

3.1. Wave data

WaveWatchIII modelled wave data was obtained for a coastal node offshore of Start Bay (Figure 1) in approximately 20m water depth. Total winter wave power was computed at each year for the period of December through March (DJFM), and subsequently split into contributions of the primary (south westerly) and secondary (easterly) directions, designated P_1 and P_2, respectively.

The wave directionality index (WDI) was computed for each winter from 1980 to 2018 using equation (1) as set out in (Wiggins et al., 2019a);

158 $$WDI = ((P_1 - P_2) - \overline{(P_1 - P_2)}) / \sigma(P_1 - P_2) \quad (1)$$

159 where $(P_1 - P_2)$ is the difference in wave power between the primary and secondary wave
160 directions, $\overline{(P_1 - P_2)}$ is the long-term mean and $\sigma(P_1 - P_2)$ is the long-term standard
161 deviation of that difference. Positive (negative) values of the WDI represent winter periods
162 where the wave climate was more southerly (easterly) than average.

163 *3.2. Atmospheric indices*

164 Winter averaged (DJFM) atmospheric index values for the station-based NAO (based on the
165 difference of normalized sea level pressure (SLP) between Lisbon, Portugal and
166 Stykkisholmur/Reykjavik, Iceland since 1864) were obtained from The Climate Data Guide
167 (downloaded from the National Center for Atmospheric Research,
168 https://climatedataguide.ucar.edu/). Additionally, values of the West Europe Pressure
169 Anomaly (WEPA) were obtained via hindcasts of SLP between s Valentia (Ireland) and
170 Santa Cruz de Tenerife (Canary Islands), as developed by Castelle et al (2017) from
171 Twentieth Century Reanalysis data (https://www.esrl.noaa.gov/psd/). Despite SLP derived
172 NAO records being available as far back as the mid to late 1800s, and proxy reconstructions
173 (described later in section 5) going even further up to 3000 years before present, records of
174 WEPA only date back to 1906 due to limited SLP records and inconsistent hindcasts beyond
175 this.

176 Previous studies along the entire length of the south coast of England (Wiggins et al., 2019b)
177 have shown that individual wave power contributions from the primary and secondary wave
178 directional modes are well correlated with WEPA and NAO respectively. Winter values of
179 the WDI for Start Bay are positively correlated with both NAO and WEPA, suggesting that a
180 combination of the two indices may improve the predictive skill at this location. To assess

this further, an empirical stepwise multiple linear regression (SMLR) model was constructed using both NAO and WEPA.

3.3. Modelled longshore sediment flux

A look-up table modelling approach was applied by McCarroll et al. (2020), for the period 1980 – 2018, to transform offshore wave conditions to breakpoint values in order to estimate alongshore wave power and potential longshore sediment flux within the Start Bay embayment. The estimated flux is 'potential' as the model assumes unlimited sediment availability. Bathymetry for the model was obtained using inshore multibeam (Wiggins et al., 2019a), combined with offshore multibeam from 2013 (UKHO, 2013). To generate the inshore wave conditions for the look-up model, Delft3D-WAVE was run in stationary mode for ~400 scenarios, covering the full range of naturally occurring boundary wave conditions. Boundary conditions for a 1980-2018 wave time series were obtained from a coarse-grid hindcast model (WaveWatchIII, Met Office). These boundary conditions were transferred to points along the 14-m depth contour using the look-up table approach. A simple refraction-shoaling parameterisation (Van Rijn, 2014) was used to transform waves from 14-m depth to the break point, with nodes at 25-m spacing. The breaking wave conditions were used to estimate alongshore wave power using linear wave theory. Alongshore sediment flux was estimated using the CERC equation (USACE, 2002), for a range of K-value coefficients (0.04 to 0.26). The output from the look-up model is a 38-year time series of longshore wave power and potential sediment flux, which was validated against prior model results and field observations (McCarroll et al., 2019). A detailed description of the model setup and forcing can be found within McCarroll et al. (2020). Total winter transport was summed for the DJFM months, and at each location, correlations were drawn between both the observed WDI and the predicted WDI.

3.4. Topographic data and rotation index

Since 2006, monthly RTK-GPS cross-shore profile surveys of Slapton Sands have been conducted by the University of Plymouth, labelled from south to north as "P1" to "P20", with average spacings of 250m (Figure 1). Pre-winter autumn and post-winter spring surveys along the length of the beach provide alongshore averaged volume change at the southern (P1 to P3) and northern (P18 to P20) ends, both of which have been shown to linearly correlate with winter values of the WDI (Wiggins et al., 2019a). A rotation index, shown in equation (2), was computed for winter change as per the methodology in Wiggins et al. (2019b), by subtracting the normalized winter volume change (dV_i) from the southern end of the beach from the northern end, such that;

$$\text{Rotation Index} = dV_i\,(north) \quad - dV_i\,(south) \tag{2}$$

Positive values of the rotation index represent periods of clockwise northwards rotation and negative values indicate winters where anti-clockwise southward rotation has occurred.

3.5. Photographic rotation index

Despite the availability of high accuracy beach surveys from 2007 onwards, prior to this date, quantitative records of beach volume change are scarce. Any surveys that have been found lack consistency in both temporal and spatial frequency as well as method. As such, metrics for beach rotation have been obtained via proxy records of historic photographs, Ordnance Survey (OS) topographic maps and limited aerial photography. For the purposes of this study, beach width at Torcross (at the southern end of the Slapton Sands embayment, Figure 1) was chosen based on the availability of historical photographs taken from the same location (a prominent headland just south of the sea wall), and the significant negative correlation between measured beach width/volume and the WDI over the period of 2007 to 2018 (Wiggins et al., 2019a). Additionally, this location of the beach was identified in Wiggins et

al. (2019a) as being indicative of beach rotation, with a significant negative correlation with the northern end of Slapton Sands, implying beach width at one end of the embayment can be used as an indicator of beach rotation. In total, 32 oblique photographs were used, taken from the same location (dating from 1875 to 2019), without the need for rectification. In addition, seven sets of aerial photography (1944 to 2017), and three geo-rectified OS maps with high and low water contours (1887, 1852 and 1983) were also used.

To assess historical changes in beach width with the limited dataset available, an integer scale of -2 ("Very Narrow") to +2 ("Very Wide") was assessed qualitatively (as shown in Figure 7), based on manual interpretation of the entire dataset, providing a simple, categorical metric of relative beach width for each dated photograph and map for this location. The range of observed beach widths was taken into account in devising the scale, from the most accreted in 1890, to most eroded in 2016.

4. Results

4.1. WDI predictions from atmospheric indices

Initial exploration of the relationships between the WaveWatchIII derived WDI (WDI_{WW3}) with NAO and WEPA, for a 38 year timeseries between 1980 and 2018 show statistically significant ($p < 0.05$) positive correlations (Figure 2); however, relative skill in predicting the WDI_{WW3} is low for both indices ($R^2 < 0.31$).

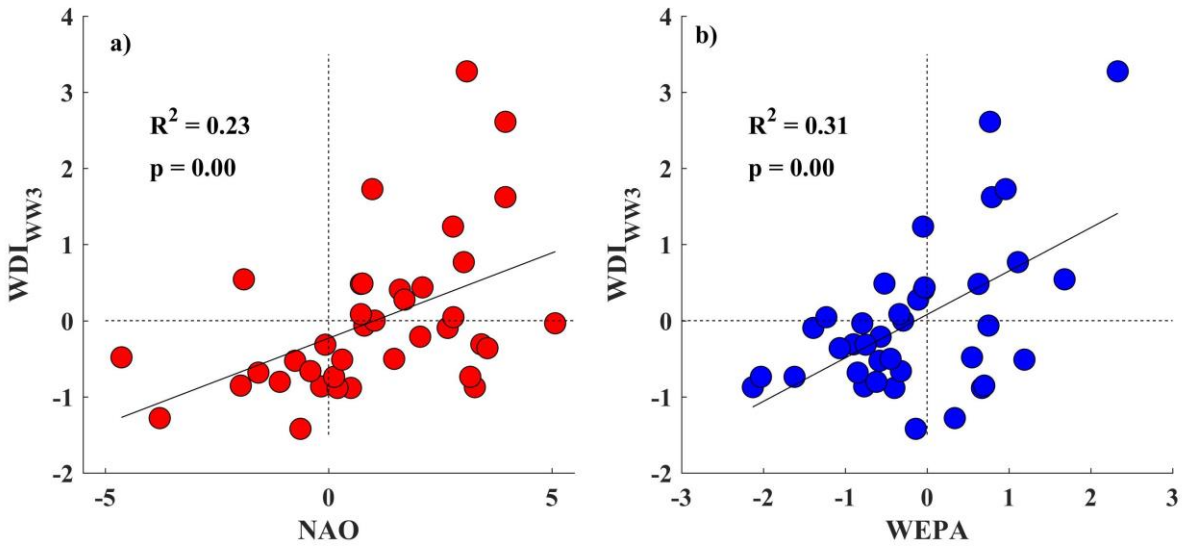

Figure 2. Correlations between winter averaged atmospheric indices NAO, WEPA and the WDI_{WW3} for the period of 1980 to 2018.

A SMLR model was created using both NAO and WEPA as predictor variables, with results suggesting that a regression model computed from a combination both NAO and WEPA variables provide improvement in the skill of predicted WDI (WDI_{Pred}). First and second order polynomial models were tested, in addition to two-term exponential regressions, with a linear fit offering the most explanatory power in predicting the WDI_{Pred}, such that;

$$WDI_{Pred} = \beta_0 + \beta_1 NAO + \beta_2 WEPA \quad (3)$$

Where β_0 represents the intercept and β_1 to β_2 are coefficients of the predictor variables, with their estimates, confidence bounds and statistics shown in Table 1.

Table 1: SMLR model statistics for the predictor variables used for modelling winter values of the WDI.

Coefficient	*Predictor*	*Estimate*	*Lower (95%)*	*Upper (95%)*	*SE*	*tStat*	*pValue*
β_0	(Intercept)	-0.19	-0.41	0.03	0.11	-1.78	0.083
β_1	NAO	0.29	0.19	0.38	0.05	6.11	5.54×10^{-7}
β_2	WEPA	0.69	0.48	0.90	0.10	6.74	8.36×10^{-8}

Overall improvements to the predictive skill of combining the indices are shown in Table 2, with the RMSE reducing from 0.9 when using NAO alone, to 0.60 when using NAO and WEPA. Similar improvements are seen when assessing the R^2 value, with an improvement of from 0.23 to 0.66 ($p = 4.71 \times 10^{-10}$). The coefficients for the two indices (Table 1) show that WEPA contributes more (0.69) to the overall predicted values of the WDI_{Pred} than NAO (0.29).

Table 2: Improvements to the SMLR models statistics for a range of input variables and sum index used for predicting winter values of the WDI_{Pred}.

Predictor Terms	***RMSE***	***R-squared***	***P-value***
NAO	0.90	0.23	2.39×10^{-3}
WEPA	0.86	0.31	3.15×10^{-4}
NAO + WEPA	0.60	0.66	5.08×10^{-9}

Outputs of WDI_{Pred} for the period of the modelled wave data (Figure 4) show the addition of both indices reproduce the winter WDI_{WW3} values with an R^2 value of 0.66.

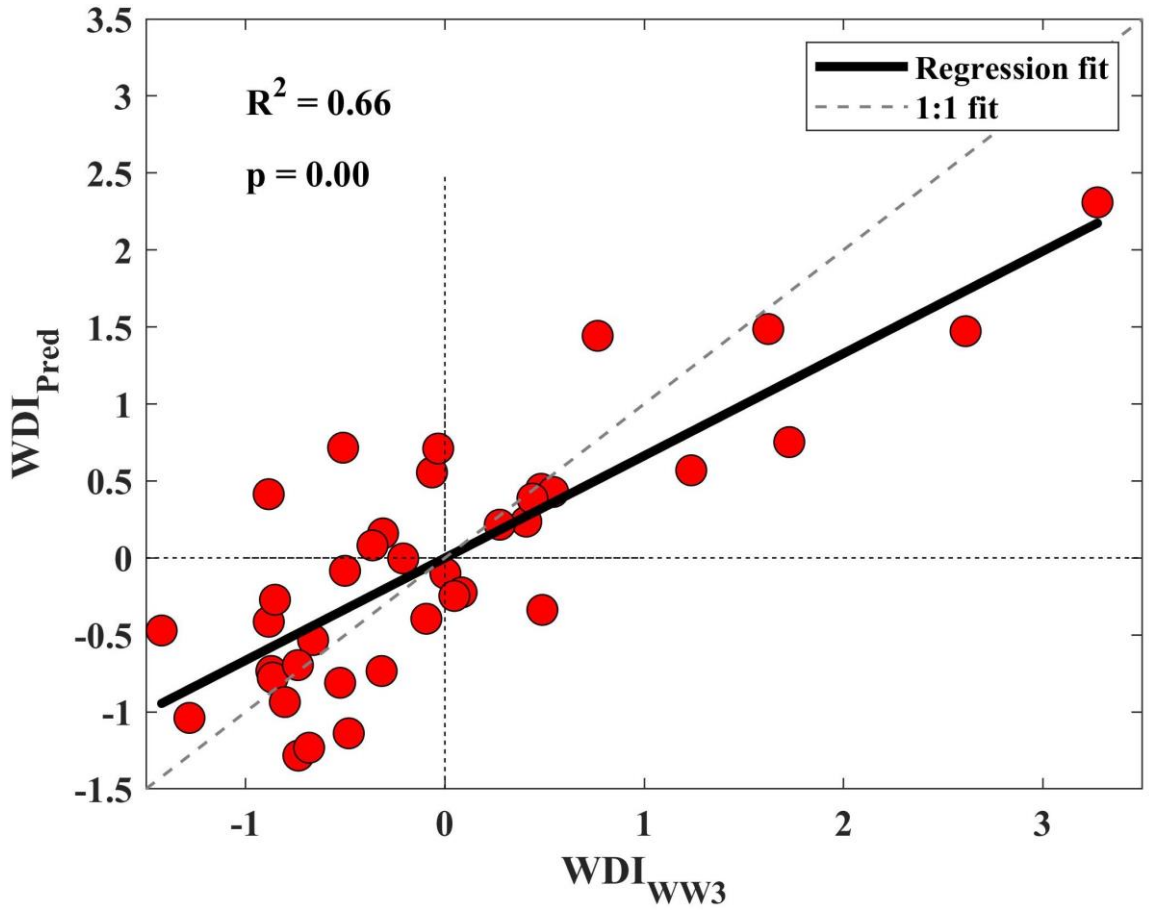

Figure 3. WDI_{WW3} for the winter periods of 1980 to 2018 plotted against WDI_{Pred} predicted using a SMLR model of winter atmospheric indices. The regression fit is shown as the bold line, whilst the 1:1 fit is displayed as the dashed grey line.

Using the regression model, values of NAO and WEPA are used to hindcast the WDI_{Pred} back to the beginning of the record of atmospheric indices (1906). The predicted output can be seen in the top panel of Figure 4, with the accumulated value of the WDI_{Pred} plotted in the middle panel.

Clear inter-annual variation can be seen within the long-term WDI_{Pred} values (Figure 4 a); however, there are periods of sustained negative or positive winter values, persisting for up to five years in a row (e.g. 2008 to 2013). Despite the high R^2 value between the WDI_{WW3} and the WDI_{Pred} hindcast from atmospheric indices (for the overlapping period of 1980 to 2018, Figure 3), there are some years where the sign of the WDI_{Pred} is opposite to the WDI_{WW3}, e.g.

2000 to 2003. This can be attributed to years where winter averaged values of NAO and WEPA are low (close to zero) or opposite in sign, leading to the larger of the two indices impacting the WDI_{Pred}. In addition, although the regression analysis was conducted using a linear relationship, the fit between winter averaged climate indices and WDI_{WW3} is not perfectly linear, especially for extremely high values of NAO and WEPA within the limited 37-year timeseries (Figure 2a and b). This explains why the regression model under predicts the value of the WDI_{Pred} for some years; however, in the majority of cases where the WDI_{WW3} is either highly positive or negative, hindcast values of the WDI_{Pred} share the same sign and are also larger in magnitude relative to the overall time series average.

The annual hindcast WDI_{Pred} values have a limited trend over the last 113 years; however, the cumulative WDI_{Pred} values (Figure 4b) show a negative trend of -0.165 yr^{-1}. Hindcast cumulative WDI_{Pred} was detrended by removing the linear mean trend using a least-squares regression, to highlight the fluctuations in the cumulative WDI_{Pred} values over time. The detrended values of the cumulative WDI_{Pred} (Figure 4c, bottom panel) indicate that there is potential periodicity in phases of positive and negative WDI_{Pred}.

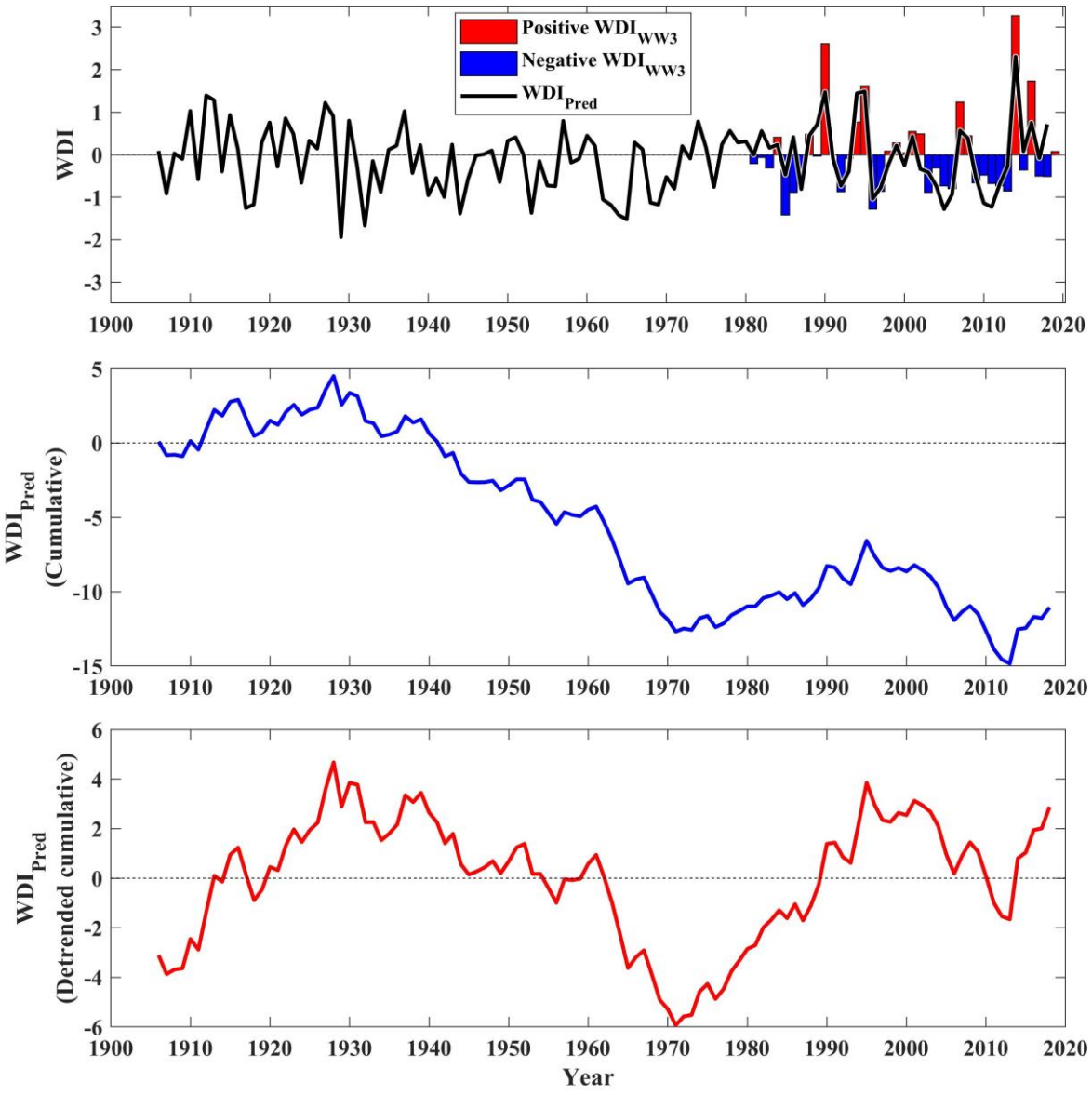

Figure 4. a) SMLR modelled WDI_{Pred} values from atmospheric indices NAO and WEPA, predicted back to 1906, as well as the values of WDI_{WW3} as obtained from the WaveWatchIII model. b) The cumulative WDI_{Pred} values from 1906 to 2018, as predicted by the SMLR model of NAO and WEPA. c) The detrended cumulative values of WDI_{Pred} from 1906 to 2018.

4.2. Modelled longshore sediment flux

To examine the relationship between the two different offshore WDI parameters (WDI_{WW3} and WDI_{Pred}) and transport rates within the embayment, potential along-shore sediment flux was computed for a series of six fixed shoreline positions (Figure 5.a), using an inshore wave

311 transformation model comprising real bathymetry (see further, McCarroll et al. (2020)). Total
312 potential winter transport totals (Figure 5.b, e, h, k, n, q) were compared with WDI_{WW3} values
313 for the period of 1980 to 2018. In all locations, significant positive correlations are observed
314 between the WDI_{WW3} and directional sediment transport (Figure 5.c, f, i, l, o, r), with the
315 strongest correlation being at Strete ($R^2 = 0.84$), the northern end of Slapton Sands (Figure
316 5.f). Other nodes located in the northern sections of the embayment show a balance of
317 northward (southward) transport under highly positive (negative) WDI_{WW3} winters, whereas
318 almost all winter WDI_{WW3} conditions drive northward transport at Hallsands in the far south
319 of the embayment.

320 The positive correlations throughout the bay suggest that the WDI_{WW3} calculated at the
321 offshore model node is an adequate proxy of the balance of inshore wave directions,
322 responsible for driving sediment transport and beach rotation within the embayment.

323

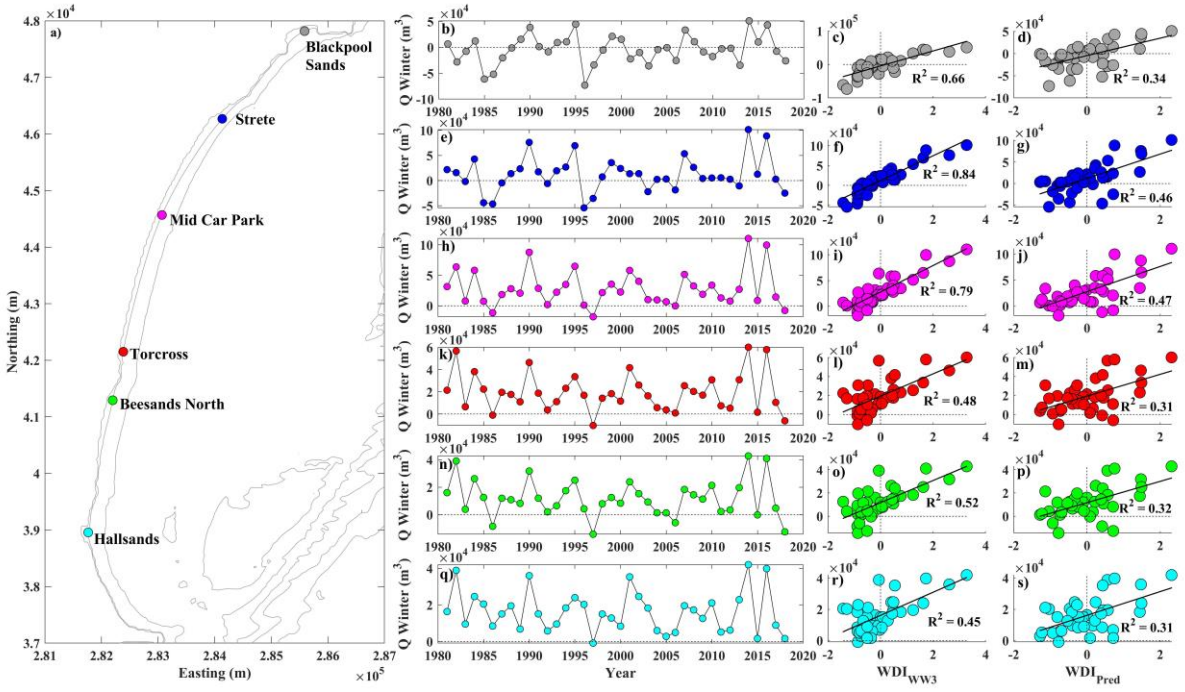

324

Figure 5. a) location map of inshore nodes at which total potential winter sediment flux has been calculated, b) total potential winter alongshore sediment flux at Blackpool Sands, e) Strete, h) Middle car park, k) Torcross, n) Beesands North and q) Hallsands. Panels c), f), i), l), o) and r) show the correlation between the WDI_{WW3}, and longshore sediment transport at the six locations, whilst panels d), g), j), m), p) and s) show the same correlations but with values of WDI_{Pred}.

In addition to the comparisons between modelled sediment transport and WDI_{WW3}, the same comparison was conducted against values of the WDI_{Pred}, as produced by the SMLR (Figure 5 d, g, j, m, p and s). At all sites, weaker but similarly positive correlations were observed, with all results being significant at the 95% confidence interval, highlighting that the WDI_{Pred} computed from climate indexes is a suitable proxy for estimating flux at the shoreline. Although the WDI_{Pred} values are consistently lower than the WDI_{WW3} (in part due to the standardized nature of the WDI wave power parameter)

4.3. Validation against beach surveys and historical records

To demonstrate the potential application of WDI_{Pred} in predicting beach rotation, correlations with contemporary and historical beach rotation are presented. Similar to previous studies of both Slapton Sands and other locations in the south west, values of the WDI_{WW3} are well correlated with the rotation index (defined in eq. 2) for the period of 2008 to 2019, derived from topographic survey data. The sign of the rotation index tracks well with the sign of WDI_{WW3} (Figure 6.a), whilst the linear correlation of the two is significant and strong ($R = 0.77$, $p = 0.00$, Figure 6.b). Similarly, the correlation between the WDI_{Pred} and rotation index is positive ($R = 0.47$), despite not being statistically significant at the 95% confidence limit; however, it is observed that the correlation is much stronger and statistically significant ($R = 0.74$, $p=0.01$), if the winter change from 2017/18 (due to a single easterly event) is removed as an outlier (discussed further in Section 5).

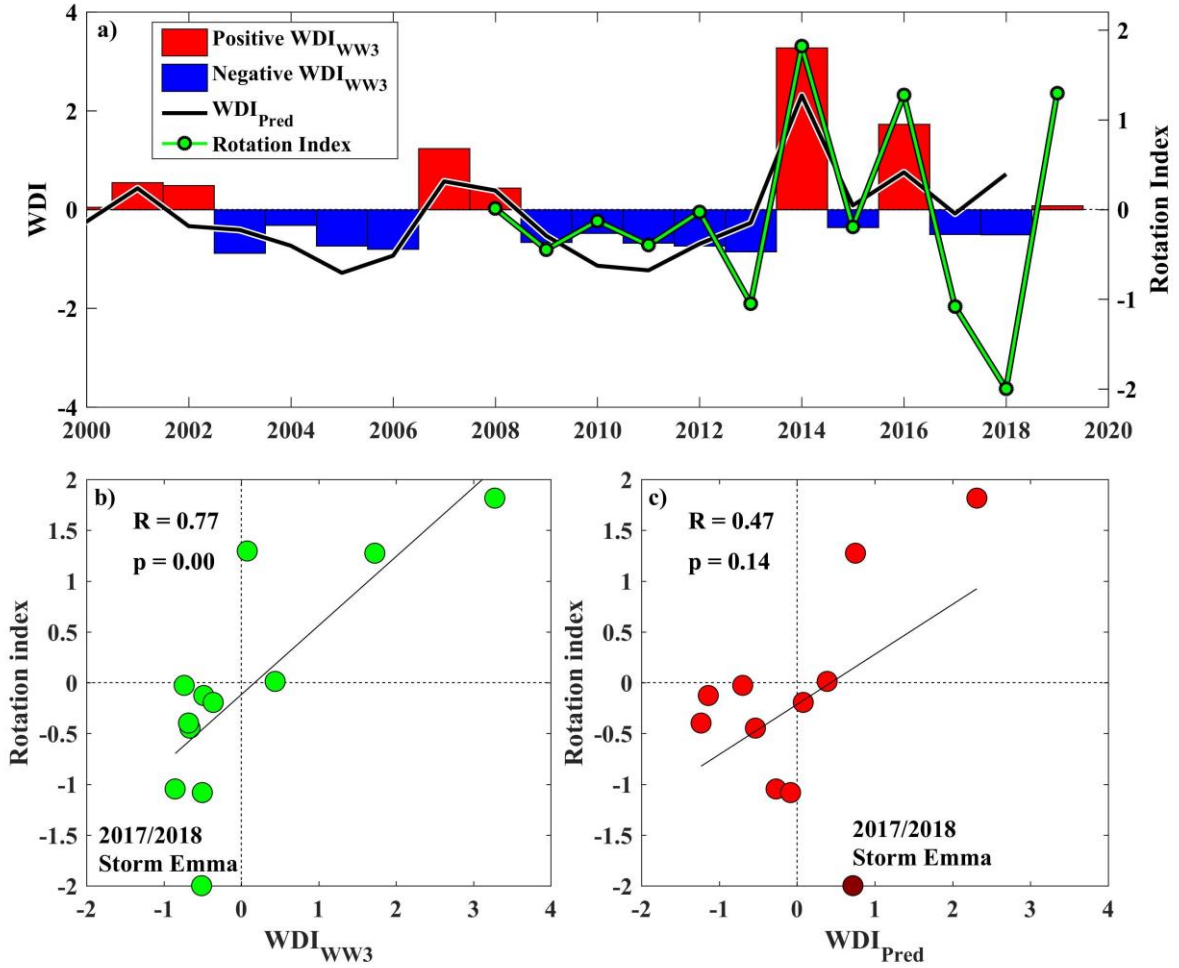

Figure 6. a) Time series of short term (~20 years) WDI_{WW3} values, shown by the red and blue bars, overlaid with WDI_{Pred} from the NAO and WEPA SMLR model, shown as the black line. The rotation index (green line) over the period of 2008 to 2019, derived from measured winter change (November to March) in beach volume at opposing ends of Slapton Sands, with positive (negative) values indicating northward clockwise (southward anticlockwise) beach rotation. b) Correlation between WDI_{WW3} and winter rotation index for the period of 2008 to 2019. c) Correlation between winter WDI_{Pred} and the winter rotation index for the period of 2008 to 2018.

The lack of consistent high-quality shoreline data before 2006 means proxy records are the only possibility for validation of the longer-term WDI_{Pred} values. Time series of the qualitative beach width assessment for Torcross and the detrended cumulative WDI_{Pred} values for the period spanning 1906 to 2019 are shown in Figure 7.a. The beach appears widest during the last decade of the 1800s, then beginning to narrow up to the 1920's, remaining a similar width in photographs and maps until around 1945. A period of beach widening then

occurs until the early 1970's, before narrowing again until 2016, the lowest beach volume in both the short-term surveys, and photo archive.

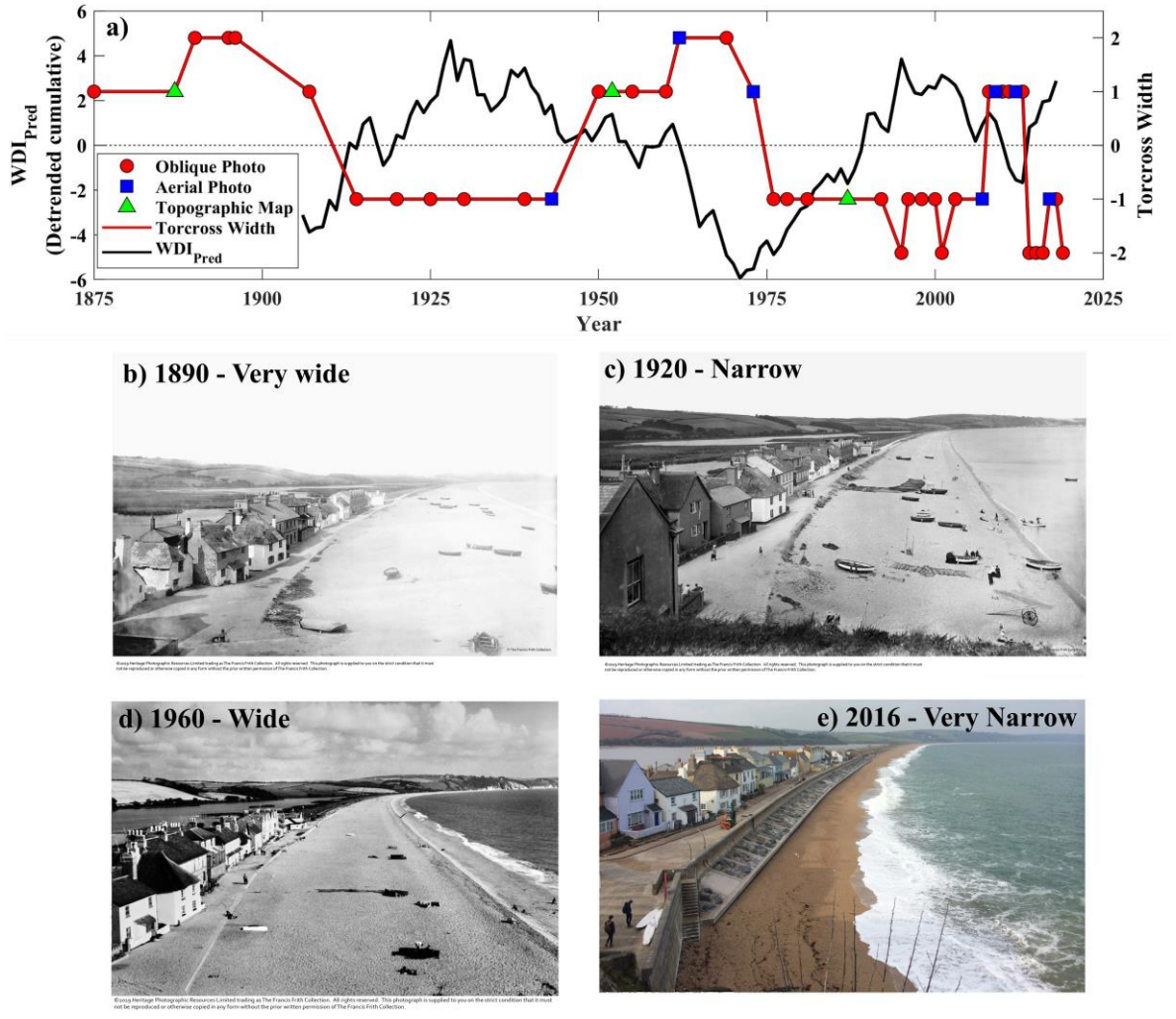

Figure 7. a) Detrended cumulative values of the WDI_{Pred} (left axis) from 1906 to 2018, overlaid on the right axis is a qualitative assessment of beach width at Torcross (southern end of Slapton Sands), with positive values indicating a wide beach, suggesting southward sediment transport and anticlockwise beach rotation, whilst negative values indicate a narrower beach, signifying a period of potential northward sediment transport and clockwise beach rotation. b) Photos of Torcross taken in 1890, c) 1920, d) 1960 (Copyright The Francis Frith Collection) e) 2016 (Copyright G. Masselink), showing different beach widths throughout the last 200 years.

Both beach width and detrended cumulative WDI_{Pred} values display low frequency fluctuations over the last 113 years, with beach width appearing to narrow during periods of

cumulative positive WDI_{Pred} and widen during sustained negative phases (Figure 7.a). Long-term detrended cumulative values for the WDI_{Pred} as well as the NAO and WEPA were computed and the results are displayed in Figure 8.

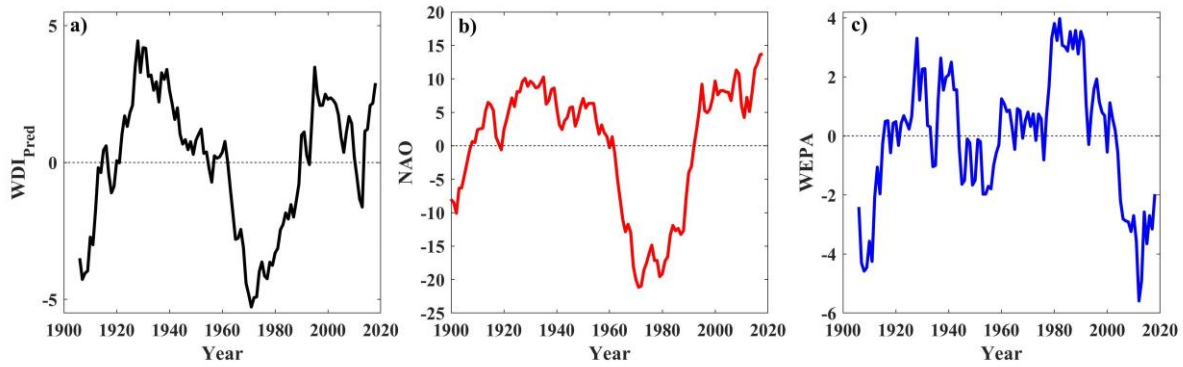

Figure 8. Detrended cumulative values of winter averaged a) WDI_{Pred}, b) NAO and c) WEPA.

For the WDI_{Pred} values (Figure 8.a), the data appears to show a multi-decadal variation in cumulative positive and negative phases, whilst the NAO (Figure 8.b) and WEPA (Figure 8.c) display similar scale variations (Figure 8.c).

5. Discussion

This study has shown that combining two major winter-averaged climate indices, NAO and WEPA, in a SMLR model significantly improves skill when trying to predict winter-averaged offshore directional wave climate (WDI), when compared to using the individual indices. Given that the WDI is key predictor of the magnitude and direction of beach rotation at this, and many similar sites along the length of the southern UK coastline (Wiggins et al., 2019b), the ability to forecast its value from two significant indices represents a step forward in assessing the accuracy in historical records of beach rotation, and the future potential to predict wave climate and morphological behaviour at seasonal to centurial timescales. Whilst previous studies have been able to link changes in atmospheric variability to deviations in wave height or direction (Barnard et al., 2015; Burvingt et al., 2018; Castelle et al., 2018,

2017; Dodet et al., 2010; Harley et al., 2017; Ranasinghe et al., 2004), the combination of multiple indices for direct calculation of a bi-directional wave climate parameter for opposing directions is unique.

Both the WDI_{WW3} and WDI_{Pred} were shown to correlate with winter integrated potential longshore transport rates throughout the embayment (McCarroll et al., 2020). Statistically significant ($p < 0.05$) correlation coefficients for WDI_{WW3} and WDI_{Pred} ranging from 0.67 to 0.92, and 0.56 to 0.68, respectively, show that the WDI calculated for a single point offshore is a robust proxy for the inshore wave climate and sediment transport. Similar to this study, significant correlations were found by Splinter et al. (2012) between yearly modelled net longshore transport rates and positive phases of the Inter-decadal Pacific Oscillation (IPO) and the Southern Oscillation Index (SOI); however, regression models combining both indices required a five-year smoothing average of both predictor and response variables, in addition to separate model equations for positive and negative phases of the IPO, incorporating different coefficients and predictor values at different time lags. The simplicity of the SMLR model used in this study, suggests that where WDI calculations are well correlated with beach rotation (Wiggins et al., 2019a, 2019b), similar analysis can be conducted at other rotation dominated sites.

The results of Section 4.3 show the rotation index of Slapton Sands (as calculated from >10 year topographic survey record) is well correlated with values of the WDI_{WW3}, but not significantly correlated with the atmospheric index based WDI_{Pred} values predicted by the model over a 10-year period of observations. Further investigation into the limited dataset showed that the winter of 2017/18 featured a large single easterly storm event (Storm Emma, further description in (McCarroll et al., 2019)) which caused a significant counter clockwise rotation of the beach at the end of the winter season (March 2nd 2018). The morphological response was observed in the anti-clockwise rotational beach record and the observed

419 negative WDI_{WW3} value (– 0.51); however, it was not reflected in the positive winter
420 averages of NAO and WEPA (0.30 and 1.17 respectively). As a result, such values of
421 atmospheric indices resulted in the model predicting a positive WDI_{Pred} value (+ 0.70),
422 suggesting a more southerly than average dominance of wave power. That winter also stands
423 out as having the highest anti-clockwise rotation index during the observational period, so its
424 impact on reducing the strength of the correlation coefficient is substantial.

425 Clearly single extreme events such as this can cause significant beach rotation and substantial
426 damage to infrastructure, and whilst the WDI_{Pred} is shown to correlate well with beach
427 rotation when the 2017/18 winter is removed from the analysis ($R = 0.74$ $p = 0.01$), ignoring
428 potential outliers of the general trend presents problems in application within a coastal
429 management setting. If a longer period of accurate morphological survey data was available,
430 better understanding of the skill and limitations of the relationship between WDI_{Pred} and
431 beach rotation could be obtained.

432 Beyond the immediate correlations between both winter WDI values and recent multi-annual
433 beach rotation, it is interesting to examine the detrended cumulative record of WDI_{Pred} as
434 conceptually it provides insights into the rotational state of the embayment. Using the SMLR
435 model a hindcast record of WDI_{Pred} shows low frequency (~60-70 years) multi-decadal
436 fluctuations over the last century (Figure 8), driven by combined changes in the cumulative
437 values of winter NAO and WEPA. Although the methodology for constructing a proxy record
438 of observed beach rotation is quantitatively limited (i.e. manual interpretation of southern
439 beach width from photography and topographic maps), it does present a qualitative coherence
440 with the periodicity in the long-term cumulative WDI_{Pred} values (Figure 7a). Temporal gaps
441 and lack of consistency in the seasonal timing of photographs may lead to aliasing of higher
442 frequency variations in beach width, but the longer-term signal presented in the historical
443 record shows a clear coherence with the detrended cumulative WDI_{Pred} values, providing

444 some validation for using detrended cumulative WDI_{Pred} in this context. Several decades of
445 the last century which show a positive phases in detrended cumulative WDI_{Pred} values (e.g.
446 1900 to 1930; sustained southerly winter waves) coincide with periods of beach narrowing
447 (clockwise rotation), whilst phases of sustained negative detrended cumulative WDI_{Pred}
448 values (e.g. 1940 to 1970; higher percentage of easterly winter waves) coincide with beach
449 widening (anti-clockwise rotation). Current improvements to shoreline detection from
450 satellite images dating back to the 1980s, could provide the extended datasets required (e.g.
451 Vos et al., 2019), and would further assist in validating regression models of atmospheric
452 indices and their control on wave climates and beach response.

453 Successive winters of the same WDI_{Pred} sign (positive or negative) may drive cumulative
454 beach rotation in a particular direction or maintain the planform shape if already rotated.
455 Event-scale wave action can cause rapid changes to the beach profile and planform shape,
456 and reversals of wave direction have been shown to quickly counter-rotate the embayment's
457 of Start Bay (McCarroll et al., 2019; Ruiz de Alegria-Arzaburu and Masselink, 2010;
458 Wiggins et al., 2019a); however, this study has identified that multi-decadal trends in the
459 detrended cumulative WDI_{Pred}, are mirrored in beach rotation proxies over the last 113 years.
460 Such multi-decadal beach rotation patterns have been identified in other locations over a
461 comparable time period, such as the south coast of Pembrokeshire, Wales, UK, with similar
462 correlations found between wave angle variations driving beach rotation under contrasting
463 phases of the NAO (Thomas et al., 2013). The longer-term trends in cumulative WDI values
464 appear to dictate the general planform state of Start Bay, indicating that within the next 100
465 years, a continued upward trend in cumulative WDI values, or a potential phase shift into a
466 sustained negative period may lead to sustained clockwise rotation or reversal and anti-
467 clockwise rotation.

To place the observed contemporary changes in context with long-term reconstructions of the NAO, detrended cumulative values of the WDI_{Pred}, NAO and WEPA from the current study are plotted on a log time scale in Figure 9. a, b, and c. For comparison, detrended cumulative values of two extened NAO reconstructions are also presented. The first (Figure 9. d), dating back to 1400, is derived from tree-ring and ice-core proxies from Cook et al. (2002)The second (Figure 9. e) is presented as a ~3000 year record of detrended cumulative normalised stalagmite growth rates (Baker et al., 2015), inverted for ease of comparison, with high growth rates representative of drier conditions, reflective of negative NAO phases.

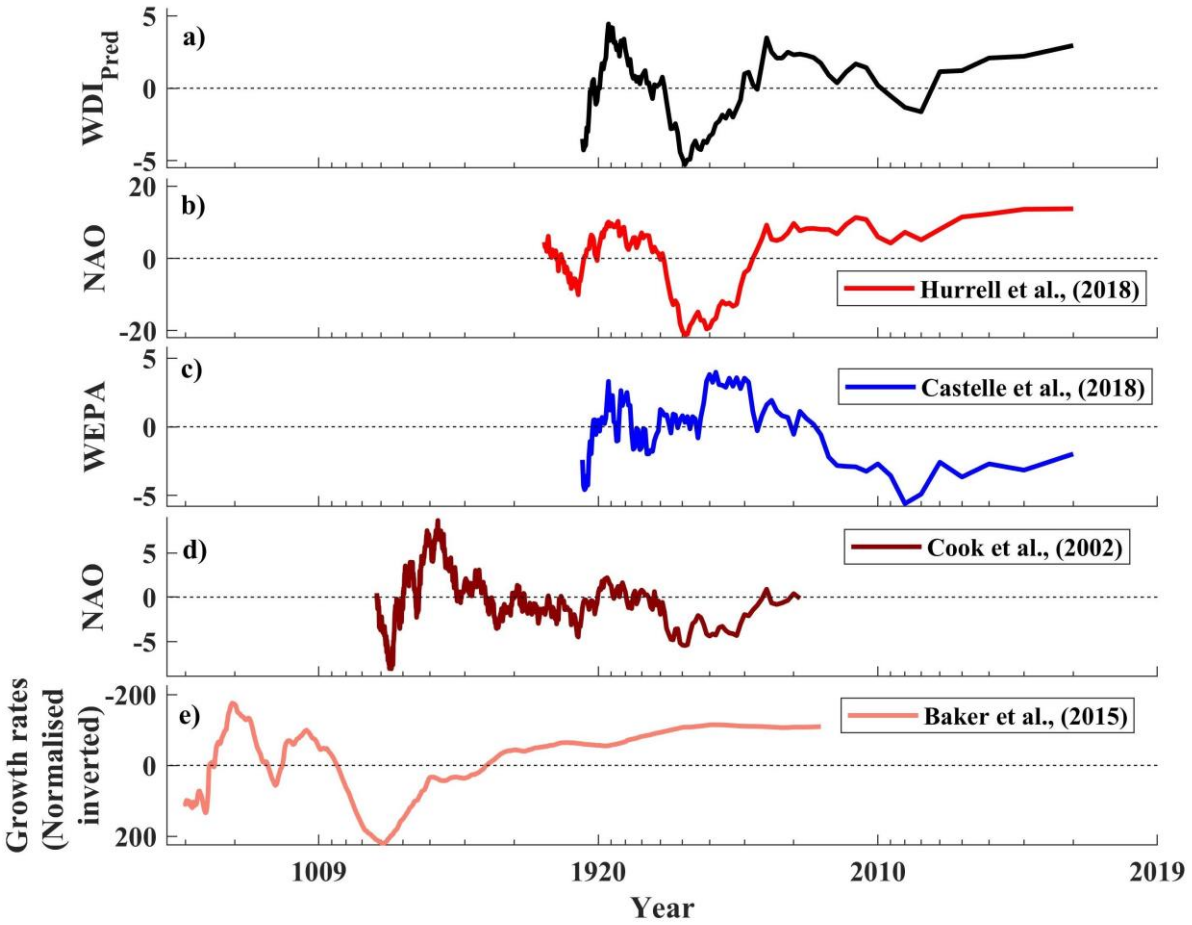

Figure 9. Detrended cumulative values of a) WDI_{Pred}, b) NAO from Hurrell et al., (2018) c) WEPA derived by Castelle et al., (2018), d) long-term NAO reconstructions from Cook et al., (2002), e) normalised stalagmite growth rates (inverted) from Baker et al., (2015). Time in year date (A.D.) is presented on a log scale.

Both additional records demonstrate sustained multi-decadal to multi-centurial phases of significant magnitude which have been confirmed by several other authors (e.g. Faust et al., 2016; Trouet et al., 2012). These observed fluctuations are of significantly greater scale and duration than those exhibited within the 113 years assessed in this study. Long-term variations in NAO have seen noticeable climate shifts identified in Europe over the last 2000 years, including a relative warming during the MCA (~800 to 1300 A.D.) due to persistent positive NAO (Trouet et al., 2009), as well as a cooler period during the LIA (~1400 – 1850 A.D.) linked to a persistent negative NAO phase (Luterbacher et al., 2002). European coastal response to these changes has been documented, with large-scale dune growth and inland sand migration evidenced during the LIA under negative NAO conditions, due to increased sand availability and stronger onshore winds (Clarke and Rendell, 2006), as well as cooler temperatures limiting vegetation growth and destabilising dunes (Jackson et al., 2019). Historical accounts of many settlements and agricultural land being abandoned due to wind driven sand migration throughout Europe (Clarke and Rendell, 2009), indicates that atmospheric effects on coastal communities have been always been apparent, driving a constant need for shoreline adaptation. Within the context of the present study site, the shoreline of Start Bay has likely undergone many previous sustained rotational states, evidenced by the loss of two historical settlements at opposing ends of the embayment (Figure 1), Strete Undercliff and Hallsands (Wiggins et al., 2017), within only the last 300 years. Exact dates of Strete Undercliff's formation are unclear, but it was well established by 1652 A.D. at the northern end of the embayment, likely following a sustained positive phase of cumulative NAO winters (Figure 10), driving clockwise rotation and northward sediment transport, resulting in a wide beach. It's eventual decline and demise 130 years later (1782 A.D.) followed an opposing phase of cumulative negative NAO winters, possibly driving anti-clockwise rotation and southward sediment transport. Around the same time, early

records of the formation of Hallsands, in the southern corner of the embayment, suggest anticlockwise rotation produced a wider beach and encouraged settlement at this location, before dredging of beach shingle (Worth, 1904) and a reversal towards more positive NAO winters at the turn of the 20th century (Wiggins et al., 2017), depleted the protective beach and the village was abandoned in 1917.

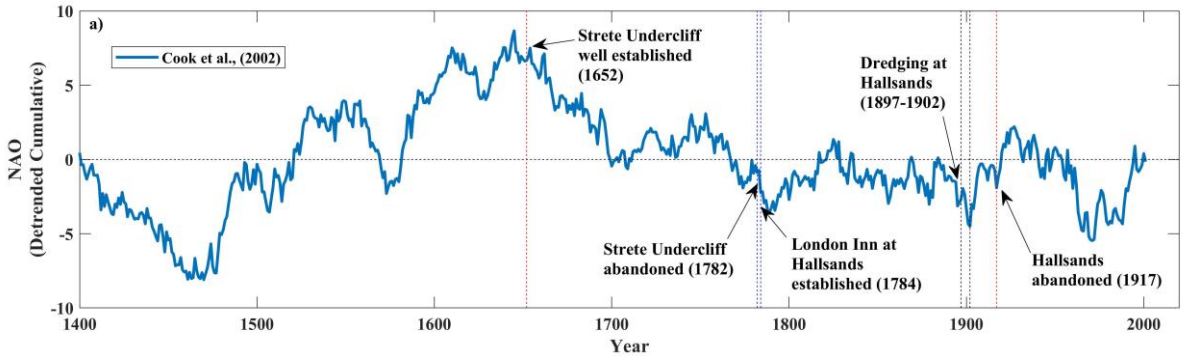

Figure 10. Detrended cumulative NAO reconstruction from Cook et al. (2002), with annotations describing the establishment and subsequent demise of two historic settlements within Start Bay, Strete Undercliff in the north, and Hallsands in the south.

The observed low frequency variations in long-term NAO suggests that sustained morphological rotations may have been occurring over substantially longer timescales in Start Bay, and much of Europe, particularly in rotation prone sites where wave climates are bi-directional.

The skill demonstrated in using combined NAO and WEPA for predicting the WDI and hence beach rotation, leads to the question of whether skilful forecasts of both indices can be obtained for either short-term (seasonal) or longer-term (multi-annual to decadal) timescales. Given that Castelle et al. (2017) have shown that NAO and WEPA are not correlated, independent forecasts of each index would need to be made well ahead of the coming winter season if the predictability of the WDI can be achieved at timescales useful to coastal managers. For example, Colman et al. (2011) made use of the NAO's positive correlation

525 with wave height in the North Sea, to predict expected operational downtime of oil and gas
526 rigs using season ahead forecasts of the NAO, made available several months in advance;
527 however, our work presents the ability, and therefore enhanced application, of predicting the
528 direction and magnitude of the wave power balance in a region where it significantly impacts
529 coastal rotation and subsequent vulnerability. Improvements to seasonal NAO forecasts are
530 currently being showcased by many authors (Baker et al., 2018; Dunstone et al., 2016; Scaife
531 et al., 2015; Wang et al., 2017); however, hindcast predictions of the NAO over the last 100
532 years has shown that forecast skill may be variable, with particular weakness during sustained
533 phases of low magnitude negative NAO winters, and better skill during the stronger, positive
534 phases during the beginning and end of the 20th century (Weisheimer et al., 2017). The results
535 of the present study and several previous research efforts (Wiggins et al., 2019a, 2019b)
536 highlight that the NAO's strong negative correlation with easterly wave events is critical in
537 the formulation of WDI values for the present location. In this case study, skilful prediction
538 of negative NAO winters is crucial for identifying the anti-clockwise rotations observed
539 during increased easterly waves. WEPA has been shown to have much greater skill in
540 predicting the occurrence of the more dominant south-westerly waves but, as yet, is largely
541 unpredictable at the season-ahead timescale, in part due to current climate models reliance on
542 accurate predictions of winter mean SLP, which are weaker for the areas around the UK and
543 Ireland (Scott et al., in prep.), leading to a lack of forecast skill in areas where NAO has little
544 influence, and WEPA is unresolved.

545 ## 6. Conclusions

546 This study has shown that a combination of two major atmospheric indices significantly
547 improves the predictive skill for a SMLR model of the bi-directional winter wave power
548 balance (WDI), which in turn has been shown to directly control morphological beach
549 rotation on shorter to multi-annual timescales. The model was then used to hindcast WDI_{Pred}

using long-term records of NAO and WEPA, with the detrended cumulative values showing periodicity linked to similar fluctuations in detrended cumulative values of both indices. Further results showed that trends in the WDI_{Pred} are mirrored in the historic records of beach rotation for this site, suggesting that beyond seasonal and event-scale rotational events, the long-term planform of this, and many similar embayments may be controlled by multi-decadal to centurial scale trends in phases of atmospheric indices.

Application of this multi-index regression method suggests that the increased ability to predict climate indices some months in advance of the coming winter period, may allow for season-ahead forecasts of forthcoming wave climates, and hence potential rotational beach impacts. Practically, this would provide coastal managers with an informed forecast of likely risks in high-impact areas, enabling proactive decisions to be made regarding hard or soft engineering works within rotational sites.

The following conclusions of this study are as follows;

1. Increased skilful prediction ($R^2 = 0.66$) of the WDI_{Pred} was be obtained from a regression model comprised of two atmospheric indices, when compared to the skill of individual indices alone.

2. Modelled alongshore wave power and potential sediment flux at fixed shoreline positions were significantly correlated with observed and predicted WDI at a range of locations within the study site; suggesting that the WDI is a valid proxy for inshore sediment transport.

3. Medium term (10-year) measured beach rotation correlates with the observed and model predicted WDI record (with the exception of an individual extreme event),

showing multiple atmospheric indices may hindcast beach rotational state at many other locations, given extensive and reliable records.

4. Longer-term records of low frequency NAO phases suggest that larger scale rotational events may have occurred at multi-centurial timescales, driving shoreline adaptation of communities in response to variations in climate indices.

Acknowledgements

This research was funded by the U.K. Natural Environment Research Council, Grant Number NE/M004996/1; BLUE-coast project.

The authors would like to thank the United Kingdom Meteorological Office, The Climate Data Guide, Bruno Castelle, Guillaume Dodet and Plymouth Coastal Observatory.

Data availability

WaveWatchIII datasets are available from the Climate index data for NAO is available at https://climatedataguide.ucar.edu/climate-data/hurrell-north-atlantic-oscillation-nao-index-station-based .Climate index data for WEPA index is available at https://www.esrl.noaa.gov/psd/data/gridded/data.20thC_ReanV2.html . Topographic survey data from Plymouth University's monthly monitoring programme is archived at the British Oceanographic Data Centre (BODC), available at https://www.bodc.ac.uk/data/ .Topographic maps are available at https://digimap.edina.ac.uk/os . Historical oblique photographs are available at https://www.francisfrith.com whilst aerial photographs can be obtained from http://southwest.coastalmonitoring.org/ .

598 **References**

599 British Broadcasting Corporation, BBC, 2016. High tide causes Torcross sea wall collapse
600 and Devon road closure. Available at: https://www.bbc.co.uk/news/uk-england-devon-
601 35558922 (Accessed: 17 October 2019).

602 Bacon, S., Carter, D.J.T., 1993. A connection between mean wave height and atmospheric
603 pressure gradient in the North Atlantic. Int. J. Climatol. 13, 423–436.
604 https://doi.org/10.1002/joc.3370130406

605 Baker, A., C. Hellstrom, J., Kelly, B.F.J., Mariethoz, G., Trouet, V., 2015. A composite
606 annual-resolution stalagmite record of North Atlantic climate over the last three
607 millennia. Sci. Rep. 5, 10307.

608 Baker, L.H., Shaffrey, L.C., Sutton, R.T., Weisheimer, A., Scaife, A.A., 2018. An
609 Intercomparison of Skill and Overconfidence/ Underconfidence of theWintertime North
610 Atlantic Oscillation in Multimodel Seasonal Forecasts. Geophys. Res. Lett. 45, 7808–
611 7817. https://doi.org/10.1029/2018GL078838

612 Barnard, P.L., Short, A.D., Harley, M.D., Splinter, K.D., Vitousek, S., Turner, I.L., Allan, J.,
613 Banno, M., Bryan, K.R., Doria, A., Hansen, J.E., Kato, S., Kuriyama, Y., Randall-
614 Goodwin, E., Ruggiero, P., Walker, I.J., Heathfield, D.K., 2015. Coastal vulnerability
615 across the Pacific dominated by El Niño/Southern Oscillation. Nat. Geosci. 8, 801.

616 Burvingt, O., Masselink, G., Russell, P., Scott, T., 2016. Beach response to consecutive
617 extreme storms using LiDAR along the SW coast of England. J. Coast. Res. 75, 1052–
618 1056. https://doi.org/10.2112/si75-211.1

619 Burvingt, O., Masselink, G., Scott, T., Davidson, M., Russell, P., 2018. Climate forcing of
620 regionally-coherent extreme storm impact and recovery on embayed beaches. Mar.

621 Geol. 401, 112–128. https://doi.org/10.1016/j.margeo.2018.04.004

622 Castelle, B., Dodet, G., Masselink, G., Scott, T., 2018. Increased Winter-Mean Wave Height,
623 Variability, and Periodicity in the Northeast Atlantic Over 1949–2017. Geophys. Res.
624 Lett. 45, 3586–3596. https://doi.org/10.1002/2017GL076884

625 Castelle, B., Dodet, G., Scott, T., 2017. A new climate index controlling winter wave activity
626 along the Atlantic coast of Europe : the West Europe Pressure Anomaly. Geophys. Res.
627 Lett. 44, 1384–1392. https://doi.org/10.1002/2016GL072379

628 Chadwick, A.J., Karunarathna, H., Gehrels, W.R., Massey, A.C., O'Brien, D., Dales, D.,
629 2005. A new analysis of the Slapton barrier beach system, UK. Proc. Inst. Civ. Eng. -
630 Marit. Eng. 158, 147–161. https://doi.org/10.1680/maen.2005.158.4.147

631 Clarke, M.L., Rendell, H.M., 2009. The impact of North Atlantic storminess on western
632 European coasts: A review. Quat. Int. 195, 31–41.
633 https://doi.org/10.1016/j.quaint.2008.02.007

634 Clarke, M.L., Rendell, H.M., 2006. Effects of storminess, sand supply and the North Atlantic
635 Oscillation on sand invasion and coastal dune accretion in western Portugal. The
636 Holocene 16, 341–355. https://doi.org/10.1191/0959683606hl932rp

637 Colman, A.W., Palin, E.J., Sanderson, M.G., Harrison, R.T., 2011. The Potential for Seasonal
638 Forecasting of Winter Wave Heights in the Northern North Sea. Weather Forecast. 26
639 (6), 1067–1074. https://doi.org/10.1175/WAF-D-11-00017.1

640 Cook, E.R., D'Arrigo, R.D., Mann, M.E., 2002. A Well-Verified , Multiproxy Reconstruction
641 of the Winter North Atlantic Oscillation. J. Clim. 15, 1754–1764.

642 Denbigh, A., 2017. The Slapton Line - Living with a Changing Coast. F. Stud. 1–4.

643 Dodet, G., Bertin, X., Taborda, R., 2010. Wave climate variability in the North-East Atlantic

644 Ocean over the last six decades. Ocean Model. 31, 120–131.
645 https://doi.org/10.1016/J.OCEMOD.2009.10.010

646 Dunstone, N., Smith, D., Scaife, A.A., Hermanson, L., Eade, R., Robinson, N., Andrews, M.,
647 Knight, J., 2016. Skilful predictions of the winter North Atlantic Oscillation one year
648 ahead. Nat. Geosci. 9, 809. https://doi.org/https://doi.org/10.1038/ngeo2824

649 Faust, J., Fabian, K., Milzer, G., Giraudeau, J., Knies, J., 2016. Norwegian fjord sediments
650 reveal NAO related winter temperature and precipitation changes of the past 2800 years.
651 Earth Planet. Sci. Lett. 435, 84–93. https://doi.org/10.1016/j.epsl.2015.12.003

652 Goodall, F., 2007. Lost Devon. Birliin Publishing.

653 Hails, J.R., 1975. Offshore Morphology and Sediment Distribution, Start Bay, Devon. Philos.
654 Trans. R. Soc. London. Ser. A, Math. Phys. Sci. 279, 221–228.

655 Harley, M.D., Turner, I.L., Kinsela, M.A., Middleton, J.H., Mumford, P.J., Splinter, K.D.,
656 Phillips, M.S., Simmons, J.A., Hanslow, D.J., Short, A.D., 2017. Extreme coastal
657 erosion enhanced by anomalous extratropical storm wave direction. Sci. Rep. 7, 6033.
658 https://doi.org/10.1038/s41598-017-05792-1

659 Hurrell, James, National Center for Atmospheric Research Staff, 2018. The Climate Data
660 Guide: Hurrell North Atlantic Oscillation (NAO) Index (Station-based). Retrieved from.
661 https://climatedataguide.ucar.edu/climate-data/hurrell-north-atlantic-oscillation-nao-
662 index-station-based.

663 Izaguirre, C., Mendez, F.J., Menendez, M., Luceño, A., Losada, I.J., 2010. Extreme wave
664 climate variability in southern Europe using satellite data. J. Geophys. Res. Ocean. 115.
665 https://doi.org/10.1029/2009JC005802

666 Jackson, D.W.T., Costas, S., Guisado-Pintado, E., 2019. Large-scale transgressive coastal

667 dune behaviour in Europe during the Little Ice Age. Glob. Planet. Change 175, 82–91.
668 https://doi.org/10.1016/j.gloplacha.2019.02.003

669 Klein, A.H.D.F., Filho, L.B., Schumacher, D.H., 2002. Short-Term Beach Rotation Processes
670 in Distinct Headland Bay Beach Systems. J. Coast. Res. 18, 442–458.
671 https://doi.org/10.2307/4299093

672 Luterbacher, J., Xoplaki, E., Dietrich, D., Jones, P.D., Davies, T.D., Portis, D., Storch, H.
673 Von, Gyalistras, D., Casty, C., Wanner, H., 2002. Extending North Atlantic Oscillation
674 reconstructions back to 1500. https://doi.org/10.1006/asle.2001.0044

675 Martínez-Asensio, A., Tsimplis, M.N., Marcos, M., Feng, X., Gomis, D., Jordà, G., Josey,
676 S.A., 2016. Response of the North Atlantic wave climate to atmospheric modes of
677 variability. Int. J. Climatol. 36, 1210–1225. https://doi.org/10.1002/joc.4415

678 Masselink, G., Castelle, B., Scott, T., Dodet, G., Suanez, S., Jackson, D., Floc'H, F., 2016.
679 Extreme wave activity during 2013/2014 winter and morphological impacts along the
680 Atlantic coast of Europe. Geophys. Res. Lett. 43, 2135–2143.
681 https://doi.org/10.1002/2015GL067492

682 Masselink, G., Scott, T., Poate, T., Russell, P., Davidson, M., Conley, D., 2015. The extreme
683 2013/2014 winter storms: hydrodynamic forcing and coastal response along the
684 southwest coast of England. Earth Surf. Process. Landforms 41, 378–391.
685 https://doi.org/10.1002/esp.3836

686 May, V.J., Hansom, J.D., 2003. Hallsands, Coastal Geomorphology of Great Britain,
687 Geological Conservation Review Series.

688 McCarroll, R.J., Masselink, G., Valiente, N.G., Wiggins, M., Scott, T., Conley, D.C., King,
689 E. V., 2020. Impact of a headland-associated sandbank on shoreline dynamics.

690 Geomorphology 355, 107065. https://doi.org/10.1016/J.GEOMORPH.2020.107065

691 McCarroll, R.J., Masselink, G., Wiggins, M., Scott, T., Billson, O., Conley, D.C., Valiente,
692 N.G., Sciences, M., Circus, D., Hill, B., 2019. High-efficiency gravel longshore
693 sediment transport and headland bypassing over an extreme wave event 1–19.
694 https://doi.org/10.1002/esp.4692

695 Nicholls, R.J., Marinova, N., Lowe, J.A., Brown, S., Vellinga, P., de Gusmao, D., Hinkel, J.,
696 Tol, R.S.J., 2011. Sea-level rise and its possible impacts given a "beyond4°C world" in
697 the twenty-first century. Philos. Trans. R. Soc. A Math. Phys. Eng. Sci. 369, 161–181.
698 https://doi.org/10.1098/rsta.2010.0291

699 Plomaritis, T.A., Benavente, J., Laiz, I., Del Río, L., 2015. Variability in storm climate along
700 the Gulf of Cadiz: the role of large scale atmospheric forcing and implications to coastal
701 hazards. Clim. Dyn. 45, 2499–2514. https://doi.org/10.1007/s00382-015-2486-4

702 Ranasinghe, R., McLoughlin, R., Short, A.D., Symonds, G., 2004. The Southern Oscillation
703 Index, wave climate, and beach rotation. Mar. Geol. 204, 273–287.
704 https://doi.org/10.1016/S0025-3227(04)00002-7

705 Robinson, A.H.W., 1961. The Hydrography of Start Bay and Its Relationship to Beach
706 Changes at Hallsands. Geogr. J. 127, 63–77. https://doi.org/10.2307/1793197

707 Ruiz de Alegria-Arzaburu, A., Masselink, G., 2010. Storm response and beach rotation on a
708 gravel beach, Slapton Sands, U.K. Mar. Geol. 278, 77–99.
709 https://doi.org/10.1016/j.margeo.2010.09.004

710 Scaife, A.A., Yu Karpechko, A., Baldwin, M., Brookshaw, A., Butler, A., Eade, R., Gordon,
711 M., Maclachlan, C., Martin, N., Dunstone, N., Smith, D., 2015. Seasonal winter
712 forecasts and the stratosphere. Atmos. Sci. Lett. 17, 51–56.

https://doi.org/10.1002/asl.598

Scott, T., Masselink, G., Hare, T.O., Saulter, A., Poate, T., Russell, P., Davidson, M., Conley, D., 2016. The extreme 2013 / 2014 winter storms : Beach recovery along the southwest coast of England. Mar. Geol. 382, 224–241. https://doi.org/10.1016/j.margeo.2016.10.011

Scott, T., Masselink, G., McCarroll, R.J., Castelle, B., Dodet, G., Saulter, A., Scaife, A.A., Dunstone, N., Atmospheric controls and long range predictability of directional waves in the United Kingdom & Ireland., Earth's Futur. Submitted.

Splinter, K.D., Davidson, M.A., Golshani, A., Tomlinson, R., 2012. Climate controls on longshore sediment transport. Cont. Shelf Res. 48, 146–156. https://doi.org/10.1016/j.csr.2012.07.018

Stranack, D., 2017. The Lost Village of Undercliff, Blackawton and Strete History Group.

Thomas, T., Phillips, M.R., Williams, a T., 2013. A Centurial Record of Beach Rotation. J. Coast. Res. 594–599. https://doi.org/10.2112/SI65-101.1

Trouet, V., Esper, J., Baker, A., Scourse, J., 2009. Persistent Positive North Atlantic Oscillation Mode Dominated the Medieval Climate Anomaly Persistent Positive North Atlantic Oscillation Mode Dominated the Medieval Climate Anomaly. https://doi.org/10.1126/science.1166349

Trouet, V., Scourse, J.D., Raible, C.C., 2012. North Atlantic storminess and Atlantic Meridional Overturning Circulation during the last Millennium: Reconciling contradictory proxy records of NAO variability. Glob. Planet. Change 84–85, 48–55. https://doi.org/10.1016/j.gloplacha.2011.10.003

UKHO, U.K.H.O., 2013. INSPIRE Portal & Bathymetry DAC [WWW Document]. Available

736 at. http//aws2.caris.com/ukho/mapViewer/map.action.

737 USACE, 2002. Shore Protection Manual. Government Printing Office, Washington, D.C.

738 van Rijn, L.C., 2014. A simple general expression for longshore transport of sand, gravel and
739 shingle. Coast. Eng. 90, 23–39.
740 https://doi.org/https://doi.org/10.1016/j.coastaleng.2014.04.008

741 Vos, K., Harley, M.D., Splinter, K.D., Simmons, J.A., Turner, I.L., 2019. Sub-annual to
742 multi-decadal shoreline variability from publicly available satellite imagery. Coast. Eng.
743 150, 160–174. https://doi.org/10.1016/j.coastaleng.2019.04.004

744 Wang, L., Ting, M., Kushner, P.J., 2017. A robust empirical seasonal prediction of winter
745 NAO and surface climate. Sci. Rep. 7, 279. https://doi.org/10.1038/s41598-017-00353-y

746 Waterhouse, R., 2009. Blackawton & Strete heritage appraisal: an archaeological history.
747 South Hams District Council, Totnes.

748 Weisheimer, Antje, Schaller, N., Reilly, C.O., Macleod, A., Palmer, T., Centre, E., Weather,
749 M., Ecmwf, F., Weisheimer, A, 2017. Atmospheric seasonal forecasts of the twentieth
750 century : multi-decadal variability in predictive skill of the winter North Atlantic
751 Oscillation (NAO) and their potential value for extreme event attribution. Q. J. R.
752 Meteorol. Soc. 143, 917–926. https://doi.org/10.1002/qj.2976

753 Wiggins, M., Scott, T., Masselink, G., Russell, P., Castelle, B., Dodet, G., 2017. The role of
754 multi-decadal climate variability in controlling coastal dynamics: re-interpretation of the
755 “Lost Village of Hallsands,” in: Proceedings Coastal Dynamics 2017. pp. 96–107.

756 Wiggins, M., Scott, T., Masselink, G., Russell, P., McCarroll, R.J., 2019a. Coastal
757 embayment rotation : Response to extreme events and climate control , using full
758 embayment surveys. Geomorphology 327, 385–403.

https://doi.org/10.1016/j.geomorph.2018.11.014

Wiggins, M., Scott, T., Masselink, G., Russell, P., Valiente, N.G., 2019b. Regionally-Coherent Embayment Rotation : Behavioural Response to Bi-Directional Waves and Atmospheric Forcing. J. Mar. Sci. Eng. 7, 116.

Worth, R.H., 1904. Hallsands and Start Bay. Devonsh. Assoc. 36, 302–346.